

# DAOS: A Multimodal In-cabin Behavior Monitoring with Driver Action-Object Synergy Dataset

Yiming Li, Chen Cai, Tianyi Liu, Dan Lin, Wenqian Wang, Wenfei Liang, Bingbing Li, and Kim-Hui Yap

**Abstract**—In driver activity monitoring, movements are mostly limited to the upper body, which makes many actions look similar. To tell these actions apart, human often rely on the objects the driver is using, such as holding a phone compared with gripping the steering wheel. However, most existing driver-monitoring datasets lack accurate object-location annotations or do not link objects to their associated actions, leaving a critical gap for reliable action recognition. To address this, we introduce the Driver Action with Object Synergy (DAOS) dataset, comprising 9,787 video clips annotated with 36 fine-grained driver actions and 15 object classes, totaling more than 2.5 million corresponding object instances. DAOS offers multi-modal, multi-view data (RGB, IR, and depth) from front, face, left, and right perspectives. Although DAOS captures a wide range of cabin objects, only a few are directly relevant to each action for prediction, so focusing on task-specific human-object relations is essential. To tackle this challenge, we propose the Action-Object-Relation Network (AOR-Net). AOR-Net comprehends complex driver actions through multi-level reasoning and a chain-of-action prompting mechanism that models the logical relationships among actions, objects, and their relations. Additionally, the Mixture of Thoughts module is introduced to dynamically select essential knowledge at each stage, enhancing robustness in object-rich and object-scarce conditions. Extensive experiments demonstrate that our model outperforms other state-of-the-art methods on our DAOS dataset.

**Index Terms**—Car cabin monitoring dataset, Action recognition, Object-augmented.

## I. INTRODUCTION

Driver action recognition has emerged as a crucial field of research with the growing demand for autonomous driving and advanced driver monitoring systems designed to enhance road safety. Accurate recognition of driver actions is vital for understanding behavior, assessing attention levels, and detecting potentially hazardous situations in real-time scenarios. Over the years, various approaches [1], [2], [3], [4], [5] have been applied to analyze driver actions based on visual features. To support research in this domain, several datasets have been introduced. Early datasets, such as DrivFace [6] and Pandora [7], focus primarily on facial expressions and head poses, while more recent datasets like Drive&Act [8] and

Yiming Li, Chen Cai, Tianyi Liu, Wenfei Liang and Kim-Hui Yap are with the School of Electrical and Electronic Engineering, Nanyang Technological University, Singapore. email: yiming008@e.ntu.edu.sg, e190210@e.ntu.edu.sg, liut0038@e.ntu.edu.sg, wenfei001@e.ntu.edu.sg, ekhyp@ntu.edu.sg. (*Corresponding author: Kim-Hui Yap*)

Dan Lin is with the College of Computer Science and Technology, Harbin Engineering University. email: danlin@hrbeu.edu.cn.

Wenqian Wang is with Singapore University of Technology and Design (SUTD), Singapore. email: wenqian\_wang@sutd.edu.sg.

Bingbing Li is with the Continental Automotive Singapore Pte. Ltd. email: bingbing.li@continental-corporation.com.

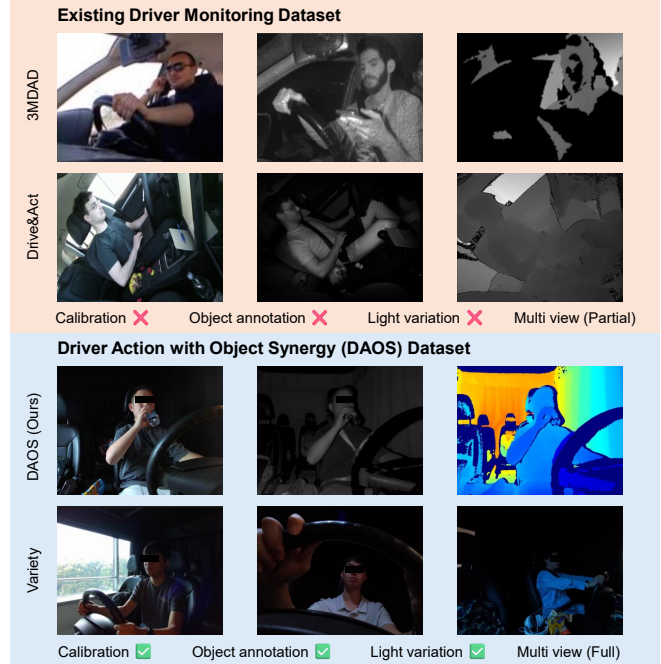


Fig. 1. Comparison of the existing Driver Monitoring dataset and our DAOS. Our dataset includes precise object annotations, multimodal calibration, various lighting conditions and multi-view videos on all three modalities.

DMD [9] have expanded in size, resolution, and multi-modal data capture. Despite these advances, accurately distinguishing visually similar driver actions within the confined car cabin remains challenging.

One of the primary challenges in driver action recognition is the restricted range of movements within car cabins, where actions are often limited to upper-body gestures such as hand movements. These gestures can appear visually similar, making it difficult to distinguish between actions based solely on visual features or posture cues. To address these challenges, recent studies [10], [11], [12], [13], [14] have incorporated additional contextual information, specifically focusing on objects in the scene that can serve as crucial indicators of driver intent. Many actions in a car cabin involve relations with specific objects, making object-based cues valuable for improving recognition accuracy.

From the perspective of video understanding systems, in-cabin driver monitoring can be viewed as a fine-grained action recognition problem under constrained spatial and temporal conditions. Unlike generic video recognition tasks, in-cabin systems must operate under strict real-time constraints, limited camera viewpoints, and dynamically changing illumination

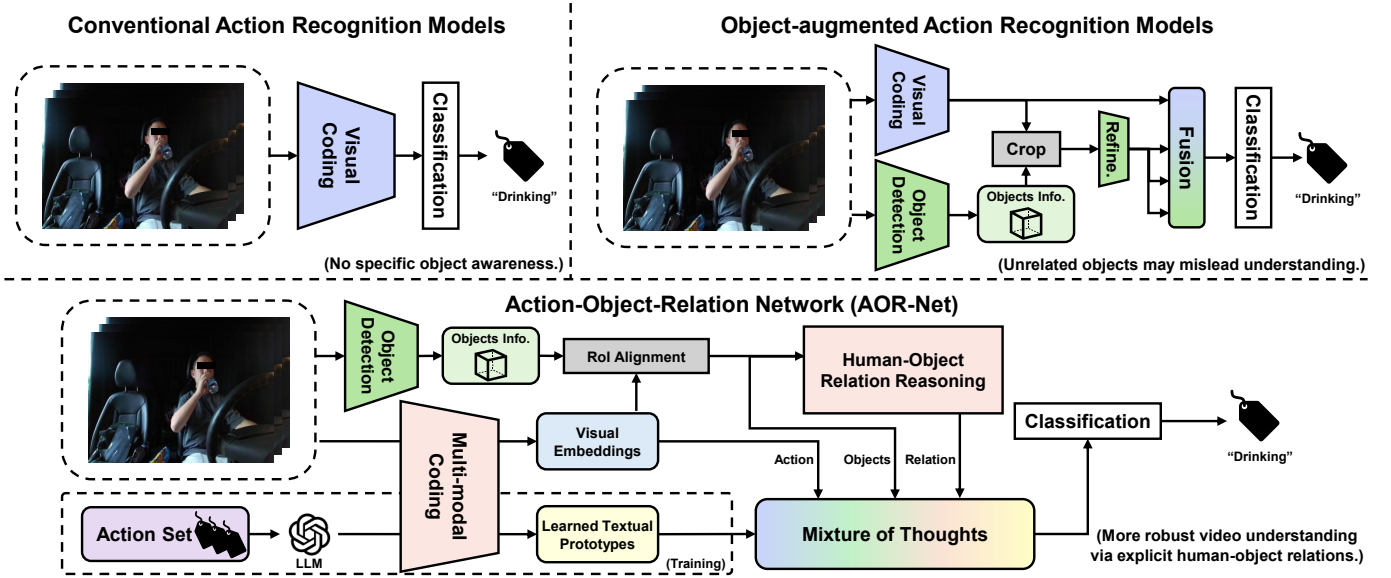


Fig. 2. Comparison of model architectures for driver action recognition. (Top left) Traditional action recognition models rely solely on visual encoders to classify actions from raw video frames, lacking object awareness. (Top right) Object-augmented action recognition models incorporate additional object information (e.g., bounding boxes or cropped regions) to enrich visual features via feature fusion. (Bottom) The proposed **Action-Object-Relation Network (AOR-Net)** further extends this paradigm by explicitly modeling human-object relations through relation reasoning and multilevel fusion Mixture-of-Thoughts (MoT), enabling a deeper understanding of driver intent in complex cabin environments.

conditions. Moreover, the cabin environment introduces additional challenges for video system design: the field of view is narrow, occlusions are frequent, and multiple sensing modalities (RGB, IR, and Depth) must be temporally synchronized to capture complementary cues about driver behavior. In practice, such systems are often deployed on embedded or in-vehicle computational units with restricted resources, which require compact, efficient, and robust video models capable of handling multi-modal fusion and temporal reasoning simultaneously. Therefore, an ideal driver monitoring system should integrate both video understanding and system-level efficiency considerations—balancing accuracy, latency, and interpretability to ensure reliable operation in safety-critical scenarios.

Although datasets such as Drive&Act [8] and DMD [9] have advanced in-cabin action research, they still lack dense, frame-level object localisation (Fig. 1). Retrofitting these benchmarks is impractical because Drive&Act and 3MDAD [15] record RGB, IR, and depth streams that are neither temporally nor spatially aligned, forcing redundant annotation for each modality. In addition, they omit many everyday interaction objects, for example cigarettes, headphones, child seats, and face masks, which are crucial for inferring driver intent.

To close both alignment and coverage gaps, we present DAOS, a fully synchronised, multi-modal, four-view cabin dataset built from scratch with exhaustive object annotations aligned to every frame and action. The DAOS dataset provides comprehensive annotations across 36 fine-grained driver actions associated with 15 object categories, including 9,787 action instances and over 2.5 million object instances. DAOS includes multi-modal, multi-view data from four perspectives (front, face, left, and right) using RGB, infrared (IR), and depth modalities, totaling over 74 hours of data. A key feature of DAOS is its precise temporal alignment of actions

and objects, enabling researchers to focus on action-related human-object relations for a deeper understanding of driver activity. This alignment creates a foundation for exploring object-augmented action recognition in complex, object-dense environments like car cabins.

Despite the recognised value of integrating object information into action-recognition frameworks, a critical review of leading models [12], [13], [14] exposes a shared limitation: insufficient modeling of the semantic coherence between object presence and human-centric context in visual scenes. This oversight injects action-irrelevant information, undermining feature extraction and overall performance. Accurately capturing these relations is essential in driver monitoring, as not all objects in the cabin are relevant to every action. A frame can contain many objects, yet only a subset relates to the driver's action. Explicitly modelling these object-action relations sharpens contextual understanding and boosts classification accuracy in both object-rich and object-scarce conditions.

To enable relation-aware action recognition, we introduce the Action-Object-Relation Network (AOR-Net) and evaluate it on the DAOS dataset. By jointly modelling object-level cues and their pairwise relations, AOR-Net directs attention to task-relevant objects and improves action discrimination. AOR-Net is built on Open-VCLIP [16] and introduces two key components: 1) a Chain-of-action Prompting Framework, which decomposes action understanding into stages of action, object, and relation reasoning; and 2) a Mixture of Thoughts (MoT) Module, which dynamically adjusts the weighting of action, object, and relation information. This dynamic weighting allows AOR-Net to adapt to diverse action types effectively, ensuring robust performance across varying conditions.

We summarize our contributions as follows:

- We introduce the DAOS dataset, a comprehensive driver

action recognition dataset that provides fine-grained alignment between actions and objects, filling a critical gap in current driver monitoring resources.

- We develop AOR-Net, a model specifically designed to leverage object and relational information for robust action recognition in car cabins.
- Extensive experiments demonstrate that AOR-Net achieves state-of-the-art performance on DAOS, validating the effectiveness of object-augmented, relation-aware action recognition in driver monitoring.

## II. RELATED WORKS

### A. Driver Monitoring Dataset

In recent years, with advancements in autonomous driving technology and driver monitoring systems, the demand for accurate driver action recognition has been rapidly increasing. To support these research needs, numerous action recognition datasets have been proposed [6], [17], [7], [8], [9], [25]. Early driving-related datasets, such as DrivFace [6], DROZY [17], and Pandora [7], addressed certain aspects of in-car research needs but also had limitations. DrivFace [6] primarily focuses on facial information, DROZY [17] on drowsiness detection, and Pandora [7] records head and shoulder poses. These datasets are limited in size, resolution, and scope, often focusing on a single body part, making it difficult to capture complex actions in the driving scenario.

As demands for accuracy and generalization in driver action recognition have increased, recent datasets, such as Drive&Act [8], DMD [9], and DriverMVT [25], have introduced higher resolution, larger sizes, and a more comprehensive focus on action recognition. For instance, the Drive&Act [8] dataset includes a wide range of fine-grained action annotations in driving-related scenarios, with data captured from five synchronized infrared (IR) views, and a multimodal camera with RGB, depth, and IR. Similarly, the DMD [9] dataset provides multi-level action annotations across various driving contexts, and the DriverMVT [25] dataset also demonstrates significant improvements in resolution and multi-modal data collection. Moreover, it includes heartbeat detection, adding an important physiological dimension to monitor the state of driver. However, while these datasets include object annotations, they often only label object categories or temporal intervals (e.g., Drive&Act [8]) and lack precise object location annotations or temporal alignment with actions. This limitation restricts their utility for research on object-augmented action recognition.

To address these issues, we present a new dataset, DAOS (Driver Action with Object Synergy) dataset, aimed at filling the current gaps in the driver monitoring field. DAOS not only increases the duration and the number of participating subjects but also offers a diverse range of action and object categories. DAOS's primary advantage lies in its precise temporal alignment of actions and objects, as well as detailed location annotations for each object, which make it better suited for supporting research on object-augmented action recognition. With DAOS, we aim to introduce new opportunities and challenges in driver behavior analysis and safety research, further advancing developments in autonomous driving and driver

monitoring technology. A comparison of dataset attributes is shown in Table. I

### B. Video-based Action Recognition and Understanding

Video-based action recognition has evolved rapidly from early convolutional models to recent transformer-based architectures that capture long-range temporal dependencies. Classical approaches such as Two-Stream CNNs [26] and 3D ConvNets (e.g., C3D [27], I3D [28]) model spatial and temporal cues jointly but suffer from limited temporal receptive fields. To improve efficiency, Temporal Shift Module (TSM) [29] introduces channel shifting operations to enable temporal modeling within 2D CNNs, achieving strong performance with lightweight computation. Similarly, Temporal Relation Networks (TRN) [30] and SlowFast Networks [31] enhance temporal reasoning by modeling multi-scale motion dynamics across frames.

With the rise of transformers, vision-based action understanding entered a new phase. TimeSformer [32] applies divided space-time attention to video tokens, enabling scalable temporal reasoning with high interpretability. ViViT [33] further extends the standard Vision Transformer (ViT) to videos through factorized temporal–spatial attention, improving representation capacity for large-scale benchmarks. Mformer [34] and Uniformer [35] integrate CNN inductive biases into transformer blocks to balance local and global modeling. Recent self-supervised methods, such as VideoMAE [36], leverage masked reconstruction to learn spatio-temporal representations without labels, offering strong pretraining benefits for downstream recognition and retrieval tasks.

Beyond classification, video action *understanding* research has expanded toward temporal grounding, reasoning, and compositional recognition. Methods like ActionCLIP [37] and X-CLIP [38] bridge vision and language via contrastive pretraining, enhancing generalization to open-vocabulary and zero-shot settings. More recently, Open-VCLIP [16] adapts vision-language models to video-level reasoning, providing a strong multimodal backbone for context-aware action recognition.

Despite the impressive progress, most existing methods are designed for general-purpose video understanding and do not explicitly account for the constrained, object-centric nature of in-cabin scenes. They often rely on large-scale motion cues or scene transitions, which are absent in driver monitoring where subtle hand-object relations dominate. This motivates our design of DAOS and AOR-Net, which emphasize fine-grained human–object relations and temporally aligned multimodal fusion tailored to real-world in-cabin systems.

### C. Object-augmented Action Recognition

Since objects in actions play a key role in determining action categories [39], there is an increasing trend to integrate object information into action-related tasks, such as action recognition and action detection [40], [41], [42].

The field of object-augmented action recognition has been advanced by several innovative models. STLT [11] advocates for the fusion of layout and appearance-based models using multi-head attention. STIN [10] explores geometric relations

TABLE I  
COMPARISON OF VISION-BASED DRIVER MONITORING DATASETS.

Attributes		Year	Size <sup>a</sup>	Subjects	F/M <sup>b</sup>	Action Annotation		Data Modality			Lighting Conditions		Camera Views	Object annotation			
Scope	Dataset					Description <sup>c</sup>	Classes	RGB	IR	Depth	Day	Night		Category	Format	Alignment	Instances
Driving-related Datasets	DrivFace [6]	2016	0.6k	4	2/2	$\times$	$\times$	640×480	$\times$	$\times$	N.A.	N.A.	1	$\times$	$\times$	$\times$	$\times$
	DROZY [17]	2016	7h	14	11/3	$\times$	$\times$	512×424	$\times$	$\times$	N.A.	N.A.	1	$\times$	$\times$	$\times$	$\times$
	Pandora [7]	2017	250k	22	10/12	$\times$	$\times$	1920×1080	$\times$	512×424	✓	N.A.	1	$\times$	$\times$	$\times$	$\times$
	DriveAHead [18]	2017	10.5h	20	4/16	$\times$	$\times$	512×424	512×424	512×424	✓	N.A.	1	$\times$	$\times$	$\times$	$\times$
	DD-Pose [19]	2019	6h	27	6/21	$\times$	13	2048×2048	2048×2048	$\times$	✓	N.A.	2	$\times$	$\times$	$\times$	$\times$
Driver Action Recognition Datasets	SEU [20]	2014	29k	20	10/10	$\times$	5	640×480	$\times$	$\times$	✓	N.A.	1	$\times$	$\times$	$\times$	$\times$
	HEH [21]	2014	N.A.	8	1/7	$\times$	19	640×480	$\times$	640×480	✓	N.A.	1	$\times$	$\times$	$\times$	$\times$
	Brain4Cars [22]	2015	2M	10	N.A.	$\times$	5	1920×1080	$\times$	$\times$	✓	N.A.	1	$\times$	$\times$	$\times$	$\times$
	NTHU-DDD [23]	2017	210k	36	18/18	$\times$	6	640×480	$\times$	$\times$	✓	✓	1	$\times$	$\times$	$\times$	$\times$
	AUC-DD [24]	2018	144k	44	15/29	$\times$	10	1920×1080	$\times$	$\times$	N.A.	N.A.	1	$\times$	$\times$	$\times$	$\times$
	3MDAD [15]	2019	24h	50	12/38	$\times$	16	640×480	$\times$	640×480	✓	✓	2	$\times$	$\times$	$\times$	$\times$
	Drive&Act [8]	2019	12h	15	4/11	$\times$	12+34	950×540	1280×1024	512×424	✓	N.A.	6	17	label	$\times$	$\times$
Datasets	DMD [9]	2020	41h	37	10/27	$\times$	13	1920×1080	1280×720	1280×720	✓	✓	3	7	label	$\times$	$\times$
	DriverMVT [25]	2022	36h	9	7/2	$\times$	3	1920×1080	$\times$	$\times$	✓	✓	2	$\times$	$\times$	$\times$	$\times$
DAOS (Ours)		2024	74h	44	10/34	✓	12+36	1920×1080	1024×1024	1024×1024	✓	✓	4	15	label + location	✓	2.58M

N.A.: information not provided by the authors. a: k and M refer to thousand and million frame numbers, h stands for hours in time. b: F for female, M for male. c: Long description of actions and relations.

between objects and subjects to enhance compositional action recognition, proving effective in generalization tasks. STRG [43] utilizes space-time region graphs and Graph Convolutional Networks, leading to notable performance gains in action recognition.

With the development of ViT, ORViT [12] integrates object-centric representations within transformer layers, using dual streams to process object appearance and dynamics, which has demonstrated significant improvements across various recognition tasks. ObjectViViT [14] employs an object-guided token sampling and attention module, optimizing performance while reducing computational load. Lastly, ObjectLearner [13] introduces a transformer model that learns object-centric summary vectors for videos, showing superior transferability to new tasks and unseen scenarios. These models collectively push the boundaries of incorporating object-level information for human action recognition. However, most of these methods do not consider the relations between certain objects and actions, which leads to the injection of unrelated object information. These models collectively push the boundaries of incorporating object-level information for human action recognition. However, most of these methods do not consider the relations between certain objects and actions, which leads to the injection of unrelated object information.

### III. DATASET

In this section, we introduce a new multi-modal, multi-view, multi-task car cabin monitoring dataset, including its collection, annotation and statistics.

#### A. Dataset Collection

To safely simulate in-cabin scenarios for action recognition, a dedicated car cabin simulator was constructed, allowing controlled data collection while safeguarding participants. The simulator setup incorporated four Azure Kinect cameras configured to capture RGB data at a resolution of 1920×1080, IR and depth data at 1024×1024, all at a frame rate of 15 fps. A curtain was used to mimic day and night scenarios, with additional LED light to simulate the lighting environment.

Our dataset includes recordings from four perspectives (front, face, left, and right) to ensure comprehensive coverage of in-cabin actions. A wide range of actions was captured, and organized into 12 coarse classes and 36 fine-grained classes, enhancing the diversity of our dataset.

Figure 4 showcases the dataset's multi-perspective and multi-modal characteristics. The left panel presents a top-down view of the data collection setup, illustrating four camera perspectives (*Left*, *Face*, *Front*, and *Right*) and their placement relative to the car cabin. These cameras captured RGB, IR, and Depth modalities simultaneously. The steering wheel and face cameras were fixed, while the cabin layout simulated a realistic vehicle with two front seats and three rear seats.

The right panel of Figure 4 shows example samples for the action *drinking*. The samples are arranged into a grid where:

- **Rows Represent Modalities:** The first, second, and third rows correspond to RGB, IR, and Depth modalities, respectively.
- **Columns Represent Perspectives:** The four columns correspond to the four camera perspectives (*Left*, *Face*, *Front*, and *Right*).

These samples highlight the dataset's comprehensive coverage of perspectives and modalities, providing diverse visual inputs for training robust models. Such multi-perspective and multi-modal setups enhance the dataset's applicability to real-world scenarios and complex tasks like object-augmented action recognition modeling.

A total of 44 participants (10 female, 34 male) contributed to the data collection. Each participant recorded two sessions of identical actions, although the sequence of actions and the position of objects varied across sessions. This variability, combined with individual differences in executing specific actions (e.g., how they pick up objects, smoke, or use a phone), increases the dataset's variety. Data collection sessions covered various times of the day and weather conditions, including sunny, cloudy, and rainy scenarios, capturing actions at the morning, noon, and afternoon intervals. This setup provides a robust dataset representing varied in-cabin scenarios, enhanc-

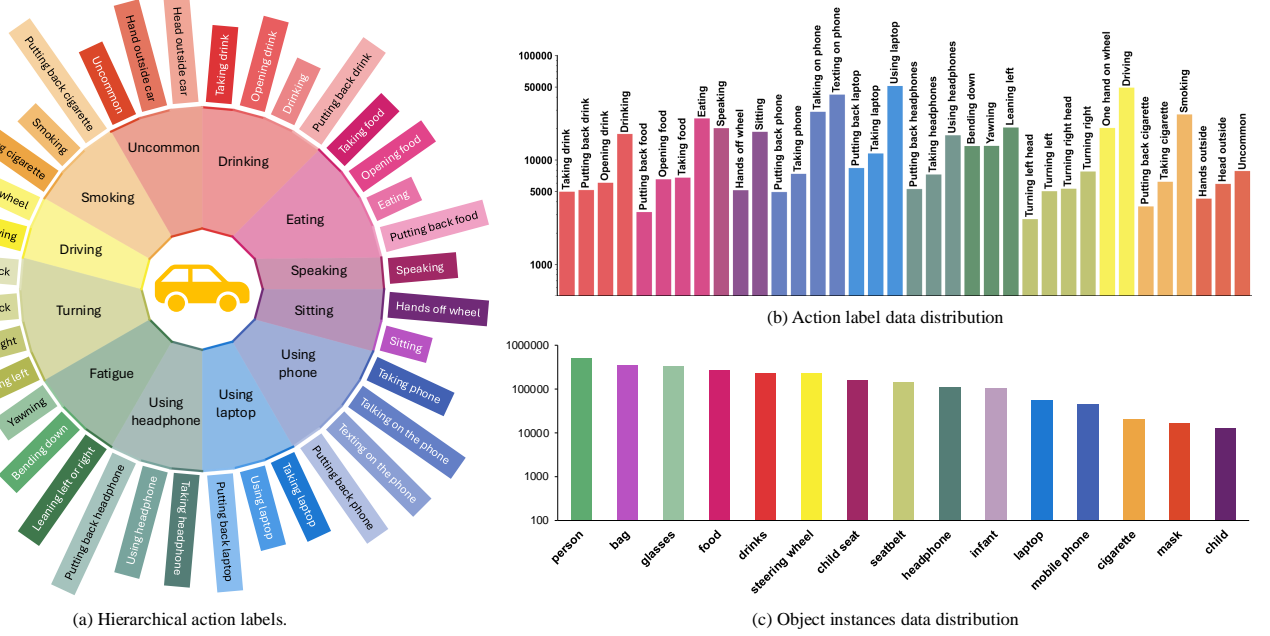


Fig. 3. Statistics of the proposed DAOS dataset. (a) Hierarchical action labels: at the coarse level, consecutive actions involving the same object are merged into 12 major categories; at the fine-grained level, those are split into 36 more detailed action classes. (b) Action label data distribution on a logarithmic scale. (c) Object instance data distribution on a logarithmic scale.



Fig. 4. Visualization and setup of the proposed DAOS dataset. (a) Car cabin setup with four Azure Kinect devices (front, facial, left, right) capturing RGB, Depth/IR under LED and NIR illumination. (b) Multimodal multiview image samples from the four camera views (Left, Facial, Front, Right) and three sensing modalities (RGB, IR, Depth).

ing generalizability and supporting diverse action recognition applications.

### B. Preprocessing and Annotation

The preprocessing of recorded data involved aligning and standardizing information across multiple modalities and camera perspectives. To achieve precise temporal synchronization between the four perspectives, Azure's external connection cables were used to synchronize across devices. For spatial alignment between the RGB and IR/depth views, each recording began with participants displaying a color checkerboard in front of the cameras. This setup provided consistent color and corner point references for calibration, allowing subsequent

alignment adjustments based on the color and geometry of the checkerboard. Furthermore, IR and depth data were converted from 16 to 8 bits, optimizing compatibility and reducing data storage demands.

**Object Annotation:** Following preprocessing, we conducted a structured manual annotation process. Object annotation was performed using CVAT (Computer Vision Annotation Tool), where keyframes with significant changes in object state were identified and annotated. The intermediate frames were then interpolated to smoothly propagate the annotations, thereby minimizing manual workload while maintaining the accuracy of the annotations across sequences.

**Action Annotation:** For action annotation, we documented

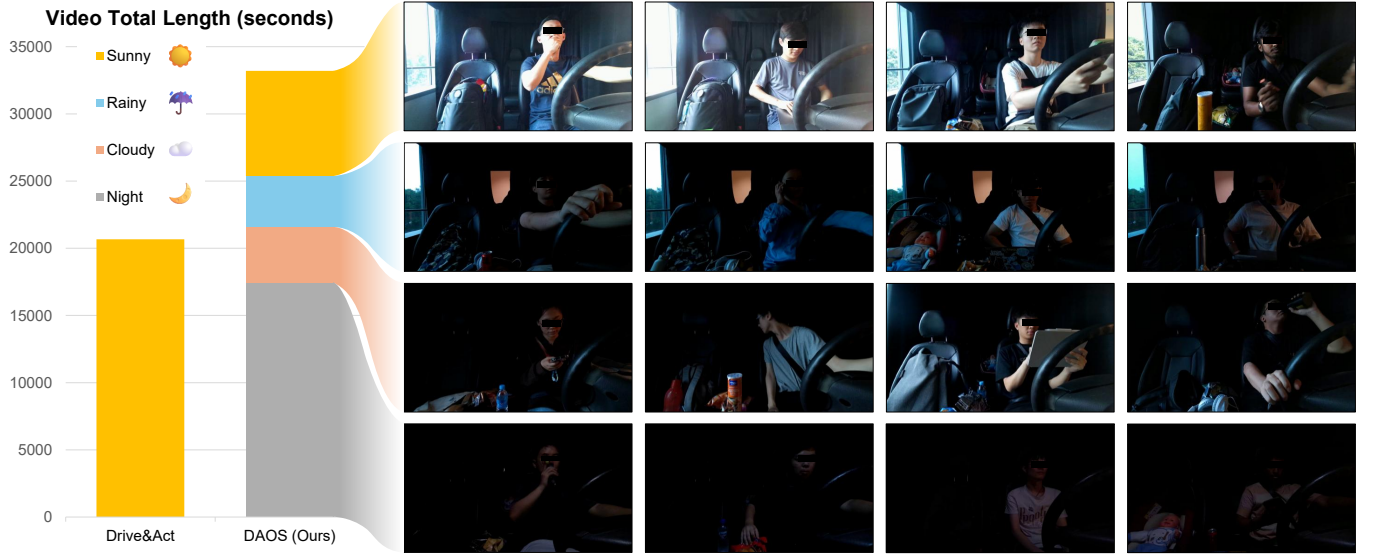


Fig. 5. Left: Data distribution comparison of lighting conditions for existing and our proposed dataset. Right: Image samples for different lighting conditions, covering sunny, rainy, cloudy and night conditions. Lighting condition settings ensures comprehensive coverage of in-cabin scenarios.

the start and end frames of each action in a structured table, allowing us to segment the data into three-second clips based on the action timestamps. This approach provides consistent action sequences for training and evaluation, enhancing the dataset's usability in action recognition models.

### C. Dataset Statistics

Our DAOS dataset comprises 74 hours of synchronized multi-modal data captured from four calibrated perspectives, totaling 9,800 annotated video segments. As Table I demonstrates, this represents a significant advancement over existing driver monitoring datasets in three key dimensions:

**Scale and Diversity:** With 44 participants (10 female, 34 male), DAOS covers 7 more subjects than the largest comparable dataset DMD [9]. The inclusion of varied lighting conditions (day/night/rain) and 36 fine-grained action categories ensures comprehensive coverage of in-cabin scenarios. As shown in Figure 5, we capture the videos across different weather and lighting conditions. A shading curtain was used to mimic day and night scenarios, with additional LED lighting to simulate the night lighting environment. The dataset's technical superiority is further evidenced by its multi-view coverage—4 synchronized perspectives versus Drive&Act's 6 unsynchronized views and DMD's 3 views.

**Multimodal Richness:** Unlike 78% of existing datasets limited to single or two modalities such as DriverMVT [25], DAOS provides synchronized RGB, IR, and depth streams. Our depth resolution (1024×1024) surpasses Drive&Act's 512×424, enabling precise 3D localization of objects and relations.

**Object-Centric Annotation:** DAOS introduces 15 object categories with 2.58 million annotated instances. Our DAOS dataset introduces pioneering object-centric annotations with label and location metadata, the first among in-cabin monitoring datasets. As Figure 3 illustrates, 64% of fine-grained

actions directly correlate with specific object states, enabling joint action-object reasoning.

The dataset includes annotations for 15 object categories. “Person” is the most frequent category, with over 500,000 annotations, reflecting its central role in interactions and actions within the car cabin. Other frequently annotated categories, such as “bag” and “glasses,” indicate their high relevance in everyday scenarios. Conversely, categories such as “child” and “mask” are less frequent, likely due to specific usage contexts or lower prevalence in the data.

From the distribution in Figure 3, we observe the following:

- **Dominant Categories:** “person,” “bag,” and “steering wheel” dominate the dataset, representing typical car cabin interactions.
- **Imbalance:** Categories such as “child” and “mask” have substantially fewer annotations, which may require data augmentation or special handling during model training to mitigate potential bias.
- **Real-World Co-occurrence:** Objects such as “bag” and “laptop” or “infant” and “child seat” often appear together in realistic scenarios, offering opportunities to model object-object relationships.

This distribution provides valuable insights into the dataset's composition and challenges for training robust models.

To ensure rigorous evaluation, we adopt a participant-wise split (Train:32, Val:6, Test:6) that prevents data leakage. This partitioning strategy, combined with the scale and annotation density of DAOS, supports novel research directions in cross-modal fusion, and occlusion reasoning through multi-view alignment, which are unrealizable with existing in-cabin datasets. Moreover, the inclusion of extensive object annotations enables support for multi-task learning and multi-modal information fusion studies, positioning our dataset as a versatile resource for advancing in-cabin action recognition research.

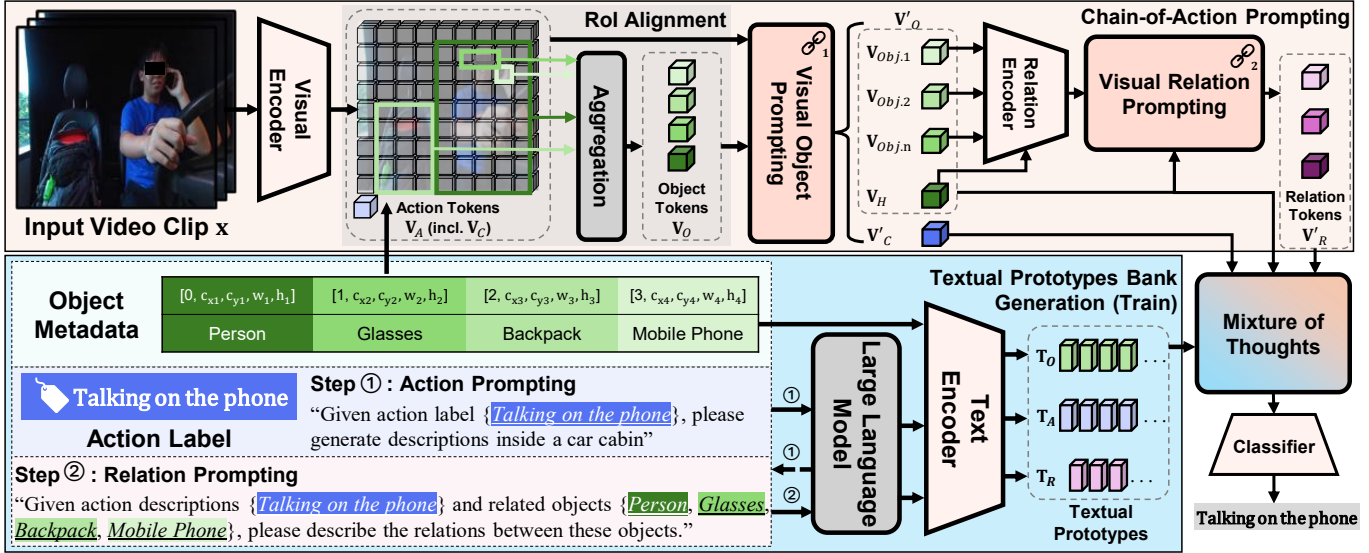


Fig. 6. An overview of the proposed AOR-Net framework. The model employs a Chain-of-action Prompting structure to sequentially extract and refine action-level, object-level, and relation-level features using attention in Object Prompting and Relation Prompting. These features are then aligned with their corresponding textual embeddings using a differentiable one-hot alignment. The Mixture of Thoughts (MoT) module dynamically adjusts the weights of these aligned features to produce the final action classification.

## IV. METHOD

### A. Preliminaries and Motivation

Recognizing driver actions in the cabin environment poses two key challenges: many actions are visually similar and can only be disambiguated by subtle object interactions, and the importance of object versus relation cues varies widely across action classes, making fixed-feature fusion suboptimal. To tackle these issues, we propose AOR-Net, built on Open-VCLIP [16], which comprises a Chain-of-action prompting (CoA) framework and a Mixture of Thoughts (MoT) module. CoA, inspired by chain-of-thought prompting [44], decomposes recognition into three sequential reasoning steps—extracting coarse action tokens, refining them with object-centric features via RoIAlign and an MLP, and then incorporating LLM-generated relation prompts to model human–object interactions (see Fig. 6). MoT addresses the drawbacks of static weighting by dynamically aligning and weighting action-, object-, and relation-level embeddings, allowing the model to emphasize the most informative cues for each action class and thereby enhance generalization. The overall AOR-Net architecture is shown in Fig. 6.

1) *Object-augmented Action Recognition (OAR)*: is designed to enhance video-based action recognition by explicitly incorporating object-level context and relations. Formally, given a video clip  $x$  and its per-frame object detections  $\{(b_i, c_i)\}_{i=1}^N$ , where each  $b_i \in \mathbb{R}^4$  is a bounding box and  $c_i$  an object class, the goal is to predict the action label  $y$ . Traditional models extract global spatio-temporal features but often fail to distinguish actions with similar motion patterns. By leveraging object appearance and location, object-augmented methods can disambiguate fine-grained actions and improve recognition robustness.

2) *Relation-prompted OAR*: Recognizing driver actions in the cabin environment poses two key challenges: many ac-

tions are visually similar and can only be disambiguated by subtle object interactions, and the importance of object versus relation cues varies widely across action classes, making fixed-feature fusion suboptimal. To tackle these issues, we propose AOR-Net, built on Open-VCLIP [16], which comprises a Chain-of-Action Prompting (CoA) framework and a Mixture of Thoughts (MoT) module. CoA, inspired by chain-of-thought prompting [44], decomposes recognition into three sequential reasoning steps: extracting coarse action tokens, refining them with object-centric features via RoIAlign and an MLP, and then incorporating LLM-generated relation prompts to model human–object interactions. MoT addresses the drawbacks of static weighting by dynamically aligning and weighting action-, object-, and relation-level embeddings, allowing the model to emphasize the most informative cues for each action class and thereby enhance generalization. The overall AOR-Net architecture is shown in Fig. 6.

### B. Chain-of-action Prompting

The Chain-of-action (CoA) prompting decomposes action understanding into three hierarchical stages: **action-level**, **object-level**, and **relation-level**. Inspired by the chain-of-thought prompting paradigm [44], which progressively reasons through intermediate steps, our AOR-Net models visual understanding as a sequential reasoning process. The model first captures coarse action cues from raw frames, then injects object-level semantics, and finally refines relational representations to infer detailed human–object interactions.

**Action-level:** Given an input video clip  $x$ , the visual encoder  $f_{\theta_V}$  of CLIP extracts a sequence of visual tokens  $\mathbf{V}_A \in \mathbb{R}^{(THW+1) \times d}$ , which includes a global class token  $\mathbf{V}_C \in \mathbb{R}^d$ . Here,  $T, H, W$  denote the temporal, height, and width dimensions of the token grid, and  $d$  represents the embedding dimension. These action-level tokens serve as the

base representation summarizing the overall spatio-temporal dynamics of the video.

**Object-level:** To enhance action representations with localized semantics, object cues are introduced at this stage. Given a set of detected bounding boxes  $\mathcal{B} \in \mathbb{R}^{TO \times 4}$  for  $O$  objects across  $T$  frames, RoIAlign [45] is applied to the spatial tokens of the visual feature map  $\mathbf{V}_A$  to extract region-specific features for each object:

$$\mathbf{v}_o^t = \text{RoIAlign}(\mathbf{V}_A^t, \mathcal{B}_o^t), \quad (1)$$

where  $\mathbf{V}_A^t$  denotes the spatial tokens at time step  $t$ , and  $\mathbf{v}_o^t$  is the corresponding object patch feature. Each cropped feature is then processed by a two-layer Multi-Layer Perceptron (MLP) followed by max pooling along the temporal dimension:

$$\mathbf{V}_O = \text{MaxPool}_t(\text{MLP}_2(\mathbf{v}_o^t)) \in \mathbb{R}^{TO \times d}, \quad (2)$$

where  $d$  denotes the shared embedding dimension between all feature levels. This operation extracts fine-grained spatial and temporal patterns for each object while maintaining temporal compactness.

To enable bidirectional information exchange between the global action context and local object cues, action and object tokens are concatenated and refined through a multi-head self-attention mechanism (MHSA):

$$[\mathbf{V}'_A; \mathbf{V}'_O] = \text{MHSA}([\mathbf{V}_A; \mathbf{V}_O]), \quad (3)$$

where  $\mathbf{V}'_A$  and  $\mathbf{V}'_O$  are the updated action and object embeddings, respectively. The MHSA operation allows each token to attend to others across the joint token set, thereby introducing global receptive fields.

As a result, object tokens gain contextual awareness of the overall scene and co-occurring actions, while action tokens learn to focus adaptively on the most relevant objects within the cabin environment. This interaction step effectively bridges coarse global motion with localized object dynamics, forming a refined representation for subsequent relational reasoning.

**Relation-level:** At this stage, human–object interactions are modeled explicitly to capture relational semantics crucial for understanding driver intent. The refined object tokens  $\mathbf{V}'_O$  are partitioned into human tokens  $\mathbf{V}_H$  and non-human object tokens  $\mathbf{V}_{Obj}$  according to their class indices. All possible human–object pairs are enumerated, and each pair’s concatenated feature is passed through a five-layer Relation Encoder implemented as an MLP:

$$\mathbf{V}_R = \text{MLP}_5([\mathbf{V}_H; \mathbf{V}_{Obj}]), \quad (4)$$

where each hidden layer has 1024 units and nonlinear activation, and the final layer projects the output back to the shared embedding dimension  $d$ . This step learns compact relation embeddings that capture interaction intensity, spatial proximity, and temporal co-occurrence between the driver and cabin objects.

To further refine these relation embeddings and enhance contextual coherence, we apply a multi-head cross-attention (MHCA) mechanism:

$$\mathbf{V}'_R = \text{MHCA}(\mathbf{Q} = \mathbf{V}_R, \mathbf{K} = \mathbf{V}'_O, \mathbf{V} = \mathbf{V}'_O). \quad (5)$$

Here, the relation tokens  $\mathbf{V}_R$  act as the query set, while the object tokens  $\mathbf{V}'_O$  serve as both keys and values.

This design allows relation tokens to selectively attend to object-level information, integrating cues about neighboring entities, occlusion patterns, and spatial configurations. Through this attention refinement, each relation token develops an adaptive understanding of the surrounding object context, enhancing discriminability for similar actions (e.g., “*picking up a phone*” vs. “*holding a phone*”) that depend on subtle relational cues.

Overall, this hierarchical prompting chain mechanism progressively transforms the representation from coarse spatio-temporal action features to semantically grounded object features, and finally to explicit human–object relational embeddings. After these stages, the enhanced visual features  $\{\mathbf{V}'_A, \mathbf{V}'_O, \mathbf{V}'_R\}$  jointly encode both global scene dynamics and fine-grained relational semantics, establishing a robust foundation for subsequent cross-modal alignment in AOR-Net.

### C. Textual Prototype Bank Generation

To construct a unified textual prototype bank aligned with multi-level visual representations, we employ the GPT-4o model to generate descriptive text for both actions and their associated human–object relations within the car cabin environment. The process consists of two main stages: (1) **action description generation** and (2) **relation description generation**, followed by an expert verification and refinement loop to ensure contextual accuracy and descriptive diversity. All validated descriptions are then encoded by the CLIP text encoder  $f_{\theta_T}$  to produce hierarchical textual features for each reasoning level, forming the final prototype bank  $\{\mathbf{T}_A, \mathbf{T}_O, \mathbf{T}_R\}$ .

1) *Action Description Generation:* For each action label  $l_A \in \mathcal{L}_A$ , GPT-4o generates textual descriptions using a cabin-aware prompt:

“Given action label {class name}, please generate descriptions inside a car cabin.”

The generated set of descriptions  $\text{desc}_A = \{d_A^1, \dots, d_A^K\}$  is evaluated by the expert verifier for contextual accuracy and diversity. If  $\text{desc}_A$  fails the validation function  $\text{Valid}(\cdot)$ , the prompt  $\text{prompt}_A$  is refined via  $\text{RefinePrompt}(\cdot)$  and regenerated. The final accepted descriptions are tokenized and encoded by the CLIP text encoder:

$$\mathbf{T}_A = f_{\theta_T}(\text{tokenize}(\text{desc}_A)) \in \mathbb{R}^{N_A \times d}. \quad (6)$$

2) *Relation Description Generation:* For each action  $l_A$ , the corresponding object set  $\mathcal{O}(l_A) \subseteq \mathcal{L}_O$  is identified, and GPT-4o generates relational sentences using the prompt:

“Given action descriptions {action description} and related objects {object names}, please describe the relations between these objects.”

The generated relation descriptions  $\text{desc}_R = \{d_R^1, \dots, d_R^M\}$  are validated by the expert verifier; if the coverage or consistency is insufficient, a refined prompt  $\text{prompt}'_R$  is used to regenerate. The approved descriptions are tokenized and encoded as relation-level textual prototypes:

$$\mathbf{T}_R = f_{\theta_T}(\text{tokenize}(\text{desc}_R)) \in \mathbb{R}^{N_R \times d}. \quad (7)$$

**Algorithm 1** Textual Prototype Bank Generation

**Require:** Action label set  $\mathcal{L}_A = \{l_A^1, \dots, l_A^{N_A}\}$ , object label set  $\mathcal{L}_O = \{l_O^1, \dots, l_O^{N_O}\}$

**Ensure:** Textual prototype bank  $\{\mathbf{T}_A, \mathbf{T}_O, \mathbf{T}_R\}$

- 1: Initialize  $\mathbf{T}_A, \mathbf{T}_O, \mathbf{T}_R \leftarrow \emptyset$
- 2: **Stage 1: Action Description Generation**
- 3: **for**  $l_A \in \mathcal{L}_A$  **do**
- 4:    $\text{desc}_A \leftarrow \text{GPT4o}(l_A, \text{prompt}_A)$
- 5:   **if**  $\neg \text{Valid}(\text{desc}_A)$  **then**
- 6:      $\text{prompt}_A \leftarrow \text{RefinePrompt}(\text{prompt}_A)$
- 7:      $\text{desc}_A \leftarrow \text{GPT4o}(l_A, \text{prompt}_A)$
- 8:   **end if**
- 9:    $\mathbf{T}_A \leftarrow f_{\theta_T}(\text{tokenize}(\text{desc}_A))$
- 10: **end for**
- 11: **Stage 2: Relation Description Generation**
- 12: **for**  $l_A \in \mathcal{L}_A$  **do**
- 13:    $\mathcal{O}(l_A) \leftarrow \text{GetObjects}(l_A, \mathcal{L}_O)$
- 14:    $\text{desc}_R \leftarrow \text{GPT4o}(l_A, \mathcal{O}(l_A), \text{prompt}_R)$
- 15:   **if**  $\neg \text{Valid}(\text{desc}_R)$  **then**
- 16:      $\text{prompt}_R \leftarrow \text{RefinePrompt}(\text{prompt}_R)$
- 17:      $\text{desc}_R \leftarrow \text{GPT4o}(l_A, \mathcal{O}(l_A), \text{prompt}_R)$
- 18:   **end if**
- 19:    $\mathbf{T}_R \leftarrow f_{\theta_T}(\text{tokenize}(\text{desc}_R))$
- 20: **end for**
- 21: **ExportToJSON**( $\text{desc}_A, \text{desc}_R$ )
- 22: **Stage 3: Object Prototype Encoding**
- 23: **for**  $l_O \in \mathcal{L}_O$  **do**
- 24:    $\mathbf{T}_O \leftarrow f_{\theta_T}(\text{tokenize}(l_O))$
- 25: **end for**
- 26: **Stage 4: Prototype Bank Assembly**
- 27:  $\mathcal{B}_T \leftarrow \{\mathbf{T}_A, \mathbf{T}_O, \mathbf{T}_R\}$
- 28: **return**  $\mathcal{B}_T$

3) *Object Prototype Encoding and Bank Assembly*: All object category labels  $l_O \in \mathcal{L}_O$  are encoded using the same text encoder:

$$\mathbf{T}_O = f_{\theta_T}(\text{tokenize}(l_O)) \in \mathbb{R}^{N_O \times d}. \quad (8)$$

Finally, all encoded features are aggregated into a structured textual prototype bank:

$$\mathcal{B}_T = \{\mathbf{T}_A, \mathbf{T}_O, \mathbf{T}_R\}. \quad (9)$$

This unified textual prototype bank provides multi-level semantic anchors for cross-modal alignment in the MoT module, enabling joint reasoning over actions, objects, and relations. The iterative generation and expert verification loop ensures that all textual prototypes are accurate, diverse, and contextually aligned with the DAOS dataset.

**D. Mixture of Thoughts (MoT)**

The in-cabin dataset contains various actions, some involving objects and others not. The relevance of object-level and relation-level information to the final classification affects the model's performance. Traditionally, a fixed weighted sum of the three levels is used to produce the final prediction. However, static weighting lacks adaptability, as object and relation importance vary significantly across action classes. To address this, we propose the MoT module, which dynamically

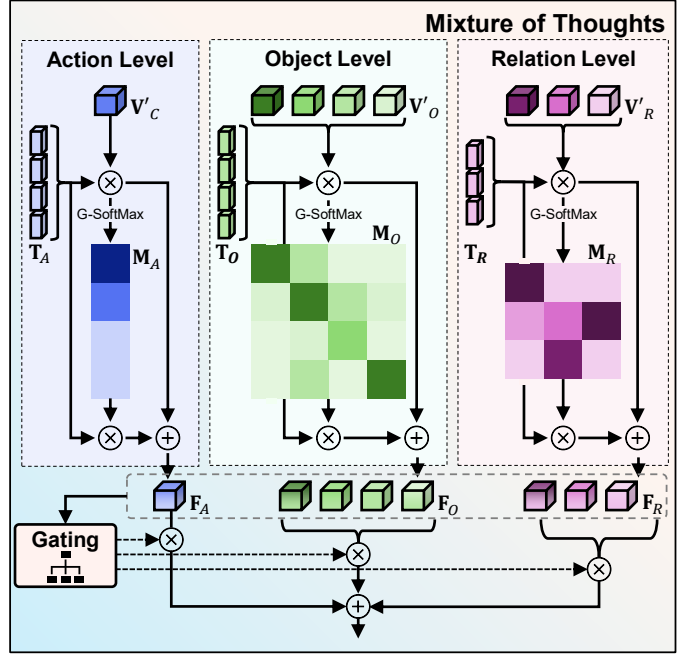


Fig. 7. Details of the Mixture of Thoughts module. The MoT module aligns these multi-level visual and textual features via a differentiable one-hot trick and dynamically fuses them to produce the final action prediction.

adjusts weights based on aligned action, object, and relation features to enhance generalization. An illustration of the MoT module is shown in Fig. 6.

First, we compute the similarity matrices between the updated visual features and their corresponding textual features for each level:  $\mathbf{M}_l = \mathbf{V}'_l \cdot \mathbf{T}_l^\top$ ,  $l \in \{A, O, R\}$ , where  $\mathbf{V}'_C, \mathbf{V}'_O, \mathbf{V}'_R$  are the updated visual features from the action, object, and relation levels, and  $\mathbf{T}_A, \mathbf{T}_O, \mathbf{T}_R$  are the corresponding textual features. We use  $\mathbf{V}'_C$  to replace  $\mathbf{V}'_A$  as an action class token.

To eliminate ambiguity in alignment, we implement the differentiable one-hot trick [46] using Gumbel Softmax for each level, as

$$\hat{\mathbf{M}}_l = \text{one-hot}(\mathbf{M}_{l, \text{argmax}}) + \mathbf{M}_l - \text{detach}(\mathbf{M}_l), \quad l \in \{A, O, R\}. \quad (10)$$

The aligned textual features are then obtained and combined with their respective visual features:  $\mathbf{F}_l = \mathbf{V}'_l + \text{MLP}(\hat{\mathbf{M}}_l \cdot \mathbf{T}_l)$ , where  $l \in \{A, O, R\}$ .

The combined features from all levels are concatenated to form the input to the MoT module. To generate dynamic weights, the MoT module flattens combined features and applies a multi-layer perceptron (MLP) followed by a softmax function shown as  $\mathbf{W} = \sigma(\text{MLP}(\text{flatten}([\mathbf{F}_A; \mathbf{F}_O; \mathbf{F}_R])))$ , where  $\mathbf{W} = [W_A, \mathbf{W}_O, \mathbf{W}_R] \in \mathbb{R}^{1+O+R}$ , with  $W_A \in \mathbb{R}$  being a scalar for the action token,  $\mathbf{W}_O \in \mathbb{R}^O$  providing weights for the object tokens, and  $\mathbf{W}_R \in \mathbb{R}^R$  providing weights for the relation tokens. The final feature representation is computed by combining the weighted features:

$$\mathbf{A}_{\text{final}} = W_A \cdot \mathbf{F}_A + \sum_{i=1}^O W_{O,i} \cdot \mathbf{F}_{O,i} + \sum_{j=1}^R W_{R,j} \cdot \mathbf{F}_{R,j}. \quad (11)$$

TABLE II  
COMPARISON OF STATE-OF-THE-ART METHODS ON FINE-GRAINED AND COARSE LEVELS OF DAOS DATASET.

Methods	Validation						Test					
	Fine-grained			Coarse			Fine-grained			Coarse		
	Top-1	Top-5	Mean-1									
ViViT-B [33]	42.36	74.12	28.90	48.46	87.96	39.22	39.47	69.43	30.35	43.24	85.14	36.22
TimeSFormer-B [32]	43.11	75.53	29.15	54.55	88.03	48.93	40.21	70.28	28.42	49.64	88.38	44.37
ORViT [12]	51.05	79.35	39.33	57.74	88.80	52.66	50.15	78.38	37.24	53.05	89.19	51.98
VideoMAE [36]	52.55	80.86	42.16	60.00	89.70	52.50	50.98	79.35	39.26	57.19	88.25	50.38
Open-VCLIP [16]	53.76	81.03	42.96	63.74	90.85	58.29	53.30	78.30	42.41	62.17	89.68	57.70
AOR-Net (Ours)	<b>55.51</b>	<b>82.50</b>	<b>45.39</b>	<b>65.73</b>	<b>92.08</b>	<b>62.60</b>	<b>55.08</b>	<b>81.99</b>	<b>44.97</b>	<b>64.49</b>	<b>90.15</b>	<b>61.68</b>
Roitberg <i>et al.</i> † [1]	58.44	86.45	50.01	62.50	92.92	61.22	54.43	78.17	42.03	60.66	89.03	56.87
Open-VCLIP† [16]	61.98	86.15	51.26	67.29	91.46	63.30	57.07	82.07	43.96	67.09	89.14	63.12
AOR-Net (Ours)†	<b>63.75</b>	<b>87.50</b>	<b>55.00</b>	<b>73.96</b>	<b>94.90</b>	<b>72.16</b>	<b>61.39</b>	<b>82.28</b>	<b>46.72</b>	<b>70.25</b>	<b>89.24</b>	<b>64.41</b>

† Results obtained using multi-modal inputs (RGB+IR+Depth).

The final prediction is produced through a fully connected layer applied to  $\mathbf{A}_{\text{final}}$ , as  $\hat{y} = \text{FC}(\mathbf{A}_{\text{final}})$ .

### E. Training and Inference

**Training Stage.** During training, our method takes video clips, action descriptions, object labels, and relation descriptions as inputs. To prevent data leakage and avoid introducing action-specific objects and relations directly into the input, we input the entire dataset’s action descriptions, object labels, and relation descriptions into the model. Both the visual and textual inputs are processed separately through the CLIP model and the CoA prompting module, resulting in updated visual features  $\mathbf{V}'_A$ ,  $\mathbf{V}'_O$ ,  $\mathbf{V}'_R$  and textual features  $\mathbf{T}_A$ ,  $\mathbf{T}_O$ ,  $\mathbf{T}_R$ . These features are then aligned and combined in the MoT module, with the final prediction obtained via a fully connected (FC) layer.

The loss function used is a cross-entropy loss. For a given sample’s final feature representation  $\mathbf{A}_{\text{final}}^n$ , the loss function is formulated as:

$$\hat{y} = \text{FC}(\mathbf{A}_{\text{final}}) \quad \mathcal{L} = -\frac{1}{N} \sum_{n=1}^N y_n \log(\hat{y}_n), \quad (12)$$

where  $N$  is the number of video samples,  $y_n$  is the ground truth label for  $n$ -th video, and  $\hat{y}_n$  is the predicted probability.

**Inference Stage.** During inference, the input process remains consistent with the training stage. The model receives the textual information for the entire dataset and generates predictions through the CoA and MoT modules, resulting in the final action classification.

## V. EXPERIMENTS

### A. Implementation Details

For training stage, we utilize the Open-VCLIP [16] model pre-trained on Kinetics-400 [47] as our backbone. We first truncate the original videos into small clips with a length of three seconds in the preprocessing process according to the video category. Then temporally sample the clips to collect 8 frames randomly, and resize the video to 224x224 followed by RandomFlip operation. The token embedding size is (2,

16, 16), and the feature dimension is 768, which aligns with Open-VCLIP. We adopt GPT-4o to enrich textual information for actions and relations. For multimodal scenarios, our AOR-Net model encodes the data of the three modalities separately and uses the MoT module to integrate and select appropriate information for prediction. Unless otherwise stated, the maximum number of objects is set to 6 by default.

All single-modality experiments are conducted using 4 NVIDIA A5000 GPUs with a batch size of 16. For multimodal experiments, the batch size is set to 4 to train the combined models end-to-end. The AdamW optimizer is utilized with a step learning rate of [10e-4, 10e-5, 10e-6] at [0, 15, 25] epochs. We train the model for 30 epochs in total using label-smoothing cross-entropy loss.

### B. Action Recognition Results

We follow previous works [8], [2] and report three standard metrics: Top-1 Accuracy (Top-1), Top-5 Accuracy (Top-5), and Mean-1 Accuracy (Mean-1). Mean-1 represents the mean of per-class Top-1 accuracy, offering a more reliable measure under class-imbalanced conditions.

Table II summarizes the results on both validation and test sets for the fine-grained and coarse-grained levels of the DAOS dataset. For fair comparison, we evaluate our AOR-Net against state-of-the-art (SOTA) transformer-based models and object-augmented methods discussed in Section II-C. For multimodal evaluation, we employ RGB, IR, and Depth modalities, training three CoA branches individually and fusing them through the MoT module. Likewise, three Open-VCLIP [16] models are fine-tuned and fused in the same manner to ensure parity.

On the **validation set**, AOR-Net achieves 55.51% Top-1 and 45.39% Mean-1 accuracy for fine-grained actions, outperforming ViViT-B and TimeSFormer-B by over 12% and 10% in Top-1 respectively. Compared with ORViT and VideoMAE, AOR-Net delivers consistent gains of +4.46% and +2.96% in Top-1, verifying the benefit of explicit relation modeling. On the coarse-grained level, it further achieves 65.73% Top-1 and 62.60% Mean-1, setting a new benchmark on DAOS. When extended to the multimodal configuration (RGB+IR+Depth,

marked by †), our model reaches 73.96% coarse-grained Top-1 and 55.00% fine-grained Mean-1, improving upon Open-VCLIP by 6.67% and 3.74%, respectively.

On the **test set**, AOR-Net maintains strong generalization, obtaining 55.08% Top-1 and 44.97% Mean-1 on the fine-grained level under the RGB setting, the best among all competing methods. Under multimodal fusion, AOR-Net achieves 61.39% Top-1 and 46.72% Mean-1 on the fine-grained task, and 70.25% Top-1 and 64.41% Mean-1 on the coarse-grained task. This surpasses the transformer-based baseline Open-VCLIP Top-1 by +4.32% and +3.16%, and remains consistently higher across all metrics compared with ORViT and VideoMAE. These improvements demonstrate that the proposed Chain-of-action (CoA) and Mixture of Thoughts (MoT) modules effectively capture fine-grained relational cues while maintaining robustness under multi-modal integration.

Overall, AOR-Net exhibits clear advantages in both single- and multi-modal settings. Its performance gains on the test set confirm the scalability and generalization of our relation-aware prompting and dynamic fusion framework, particularly in handling complex, object-driven driver behaviors in the DAOS dataset.

### C. Ablation Study

We systematically validate our architecture through three key experiments. We present visualizations of attention maps for better understanding as shown in Fig.8. Each component’s contribution is analyzed as follows:

**Maximum object number in CoA Prompting.** Table III reveals the impact of maximum object retention per frame. Setting  $\mathcal{O}=6$  achieves optimal performance with 55.51% Top-1 and 45.39% Mean-1 accuracy. Comparatively,  $\mathcal{O}=4$  reduces Top-1 by 1.57% due to insufficient object context, while  $\mathcal{O}=8/10$  introduces noise from irrelevant objects, decreasing Top-1 by 0.52-0.75%. This demonstrates our approach’s effectiveness in balancing critical feature preservation with noise suppression.

TABLE III  
ABLATION STUDY OF DIFFERENT NUMBERS OF MAXIMUM OBJECTS PER FRAME.

# Max Object ( $\mathcal{O}$ )	Metrics		
	Top-1	Top-5	Mean-1
4	53.94	81.62	43.11
<b>6</b>	<b>55.51</b>	<b>82.50</b>	<b>45.39</b>
8	54.99	81.62	42.98
10	54.76	80.21	41.26

**Effectiveness of different modules.** As shown in Table IV, our baseline achieves 53.76% Top-1 accuracy. The CoA Prompting alone boosts performance by 0.93%, demonstrating its effectiveness in modeling dynamic object relations. When combined with Mixture of Thoughts (MoT), we observe further improvements of 1.75% Top-1 and 2.43% Mean-1, indicating complementary benefits between structured reasoning (CoA) and multi-perspective fusion (MoT).

TABLE IV  
ABLATION STUDY OF DIFFERENT SETTINGS OF MODULES COMPARED WITH BASELINE. COA AND MOT STAND FOR COA PROMPTING AND MIXTURE OF THOUGHTS, RESPECTIVELY.

Modules	Metrics		
	Top-1	Top-5	Mean-1
Base	53.76	81.03	42.96
+ CoA	54.69	81.62	43.76
+ CoA + MoT	<b>55.51</b>	<b>82.50</b>	<b>45.39</b>

**Gumbel Softmax Parameters Ablation.** Table V shows that incorporating Gumbel Softmax improves discrete alignment over the normal softmax baseline. Performance gradually increases as the temperature  $T$  rises from 0.1 to 5.0, reaching the best result at  $T=5.0$  (Top-1: 55.51%, Top-5: 82.50%, Mean-1: 45.39). Extremely small or large temperatures lead to unstable gradients or overly uniform sampling, confirming that a moderate range ( $T \approx 1-5$ ) provides the optimal trade-off between stochasticity and stability.

TABLE V  
ABLATION STUDY OF GUMBEL SOFTMAX SETTINGS.

Settings	Metrics		
	Top-1	Top-5	Mean-1
Normal Softmax	53.65	80.13	42.00
T=0.1	52.46	80.73	41.65
T=0.5	54.17	80.13	42.01
T=1.0	54.76	80.65	42.19
T=2.0	53.35	81.18	44.97
<b>T=5.0</b>	<b>55.51</b>	<b>82.50</b>	<b>45.39</b>
T=10	54.49	81.79	43.76
T=50	52.55	80.38	42.19
T=100	52.79	80.17	42.75

TABLE VI  
ABLATION STUDY OF RELATION ENCODER SETTINGS.

Layers	Dim	Metrics		
		Top-1	Top-5	Mean-1
Simple Addition		54.17	80.65	42.19
L=1	d=512	54.02	80.13	42.33
L=2	d=512	54.91	<u>81.99</u>	43.49
L=5	d=256	53.93	80.69	43.06
<b>L=5</b>	<b>d=512</b>	<b>55.51</b>	<b>82.50</b>	<u>45.39</u>
L=5	d=1024	54.56	80.31	42.25
L=8	d=512	<u>55.08</u>	81.24	42.69
L=10	d=512	53.93	80.75	<b>45.56</b>

**Relation Encoder Parameters Ablation.** As summarized in Table VI, deeper relation encoders consistently enhance

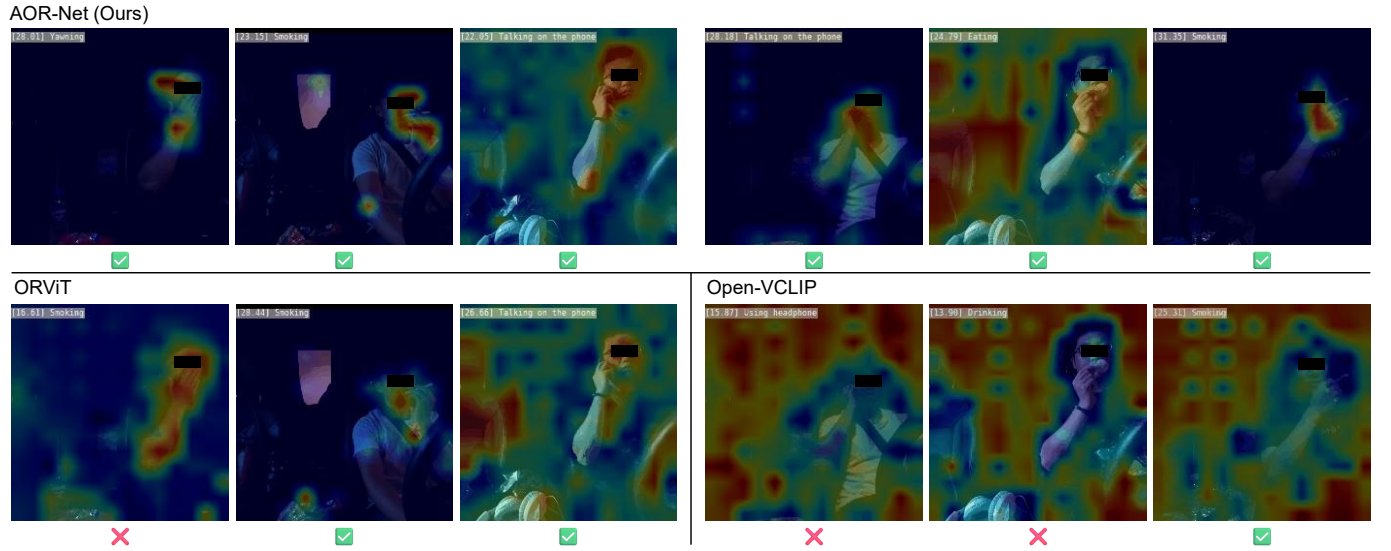


Fig. 8. Comparative visualization of attention maps from different models in the last ViT layer. Check mark stands for correct prediction and cross mark means wrong predictions.

performance up to five layers, after which accuracy saturates. The best configuration ( $L=5$ ,  $d=512$ ) achieves the highest Top-1 accuracy of 55.51%, while shallower or excessively wide networks show marginal gains or even degradation. These results indicate that moderate depth and embedding dimension yield the most effective relational representation for action understanding.

**Cross-Dataset Ablation on Drive&Act Subset.** We restrict comparisons to an RGB-only subset of Drive&Act, for which we manually annotated dense object labels, as full-object annotation across the entire dataset was infeasible. As Table VII shows, AOR-Net achieves 77.67% Top-1 (versus 76.49% for Open-VCLIP), validating the effectiveness of our CoA and MoT modules on cross-dataset evaluation.

TABLE VII  
COMPARISON RESULTS ON DRIVE&ACT [8] SUBSET.

Methods	Metrics		
	Top-1	Top-5	Mean-1
ORViT [12]	73.75	93.47	62.15
Open-VCLIP [16]	76.49	94.06	65.26
<b>AOR-Net</b>	<b>77.67</b>	<b>96.22</b>	<b>66.90</b>

**Multimodal fusion analysis.** Table VIII demonstrates progressive improvements through modality integration. Single modality shows RGB’s advantage in Top-1 (55.51%) versus Depth’s strength in Mean-1 (48.62%). Dual modality combinations achieve 4.80% Top-1 gains, with RGB+Depth reaching 60.31%. The full RGB+IR+Depth configuration peaks at 63.75% Top-1, showing 13% relative improvement over RGB alone. This 9.61% Mean-1 gap confirms the effectiveness of our MoT module in combining multimodal cues.

**Visualizations.** According to Figure 8, our model can predict most of the object-related classes correctly with explainable attention weights. Compared to existing object-augmented methods like ORViT [12], AOR-Net can suppress

TABLE VIII  
ABLATION STUDY OF SINGLE- AND MULTI-MODALITY MODEL ON FINE-GRAINED LEVEL DATA.

Modalities	Metrics		
	Top-1	Top-5	Mean-1
RGB	55.51	82.50	45.39
IR	53.23	81.35	43.51
Depth	54.58	83.54	48.62
RGB+IR	61.15	85.73	50.89
RGB+Depth	60.31	84.90	51.22
IR+Depth	60.31	86.67	50.68
RGB+IR+Depth	63.75	87.50	55.00

the influence of irrelevant objects and background information. Unlike traditional action recognition methods (Open-VCLIP [16]) without the help of additional object information, AOR-Net can focus on related objects to predict the action correctly.

## VI. CONCLUSION

We propose a multi-modal Driver Action with Object Synergy (DAOS) dataset and Action-Object-Relation network (AOR-Net). DAOS consists of over 74 hours raw videos, including 12 coarse and 36 fine-grained action classes. Using our proposed Chain-of-action Prompting and Mixture of Thoughts module, information from different levels can be organized and selected properly. Through extensive experiments on DAOS, we observed that AOR-Net achieves state-of-the-art results and verified the effectiveness of our proposed modules and architecture. It is worth noting that our model can be adapted to any CLIP-based action recognition model. However, we have not invested in the generalization ability of the model and left it for follow-up research.

## REFERENCES

[1] A. Roitberg, K. Peng, Z. Marinov, C. Seibold, D. Schneider, and R. Stiefelhagen, "A comparative analysis of decision-level fusion for multimodal driver behaviour understanding," in *2022 IEEE intelligent vehicles symposium (IV)*. IEEE, 2022, pp. 1438–1444.

[2] D. Lin, P. H. Y. Lee, Y. Li, R. Wang, K.-H. Yap, B. Li, and Y. S. Ngim, "Multi-modality action recognition based on dual feature shift in vehicle cabin monitoring," *arXiv preprint arXiv:2401.14838*, 2024.

[3] X. Wang, W. Ye, Z. Qi, G. Wang, J. Wu, Y. Shan, X. Qie, and H. Wang, "Task-aware dual-representation network for few-shot action recognition," *IEEE Transactions on Circuits and Systems for Video Technology*, vol. 33, no. 10, pp. 5932–5946, 2023.

[4] R. Wang, C. Cai, W. Wang, J. Gao, D. Lin, W. Liu, and K.-H. Yap, "Cm 2-net: Continual cross-modal mapping network for driver action recognition," in *2024 IEEE International Conference on Image Processing (ICIP)*. IEEE, 2024, pp. 2236–2242.

[5] R. Wang, W. Wang, J. Gao, D. Lin, K.-H. Yap, and B. Li, "Multifuser: Multimodal fusion transformer for enhanced driver action recognition," in *2024 IEEE 26th International Workshop on Multimedia Signal Processing (MMSP)*. IEEE, 2024, pp. 1–6.

[6] K. Diaz-Chito, A. Hernández-Sabaté, and A. M. López, "A reduced feature set for driver head pose estimation," *Applied Soft Computing*, vol. 45, pp. 98–107, 2016.

[7] G. Borghi, M. Venturelli, R. Vezzani, and R. Cucchiara, "Poseidon: Face-from-depth for driver pose estimation," in *Proceedings of the IEEE conference on computer vision and pattern recognition*, 2017, pp. 4661–4670.

[8] M. Martin, A. Roitberg, M. Haurilet, M. Horne, S. Reiß, M. Voit, and R. Stiefelhagen, "Drive&act: A multi-modal dataset for fine-grained driver behavior recognition in autonomous vehicles," in *Proceedings of the IEEE/CVF International Conference on Computer Vision*, 2019, pp. 2801–2810.

[9] J. D. Ortega, P. N. Cañas, M. Nieto, O. Otaegui, and L. Salgado, "Challenges of large-scale multi-camera datasets for driver monitoring systems," *Sensors*, vol. 22, no. 7, p. 2554, 2022.

[10] J. Materzynska, T. Xiao, R. Herzig, H. Xu, X. Wang, and T. Darrell, "Something-else: Compositional action recognition with spatial-temporal interaction networks," in *Proceedings of the IEEE/CVF conference on computer vision and pattern recognition*, 2020, pp. 1049–1059.

[11] G. Radevski, M.-F. Moens, and T. Tuytelaars, "Revisiting spatio-temporal layouts for compositional action recognition," *arXiv preprint arXiv:2111.01936*, 2021.

[12] R. Herzig, E. Ben-Avraham, K. Mangalam, A. Bar, G. Chechik, A. Rohrbach, T. Darrell, and A. Globerson, "Object-region video transformers," in *Proceedings of the ieee/cvf conference on computer vision and pattern recognition*, 2022, pp. 3148–3159.

[13] C. Zhang, A. Gupta, and A. Zisserman, "Is an object-centric video representation beneficial for transfer?" in *Proceedings of the Asian Conference on Computer Vision*, 2022, pp. 1976–1994.

[14] X. Zhou, A. Arnab, C. Sun, and C. Schmid, "How can objects help action recognition?" in *Proceedings of the IEEE/CVF Conference on Computer Vision and Pattern Recognition*, 2023, pp. 2353–2362.

[15] I. Jegham, A. B. Khalifa, I. Alouani, and M. A. Mahjoub, "A novel public dataset for multimodal multiview and multispectral driver distraction analysis: 3mdad," *Signal Processing: Image Communication*, vol. 88, p. 115960, 2020.

[16] Z. Weng, X. Yang, A. Li, Z. Wu, and Y.-G. Jiang, "Open-VCLIP: Transforming CLIP to an open-vocabulary video model via interpolated weight optimization," in *Proceedings of the 40th International Conference on Machine Learning*, ser. Proceedings of Machine Learning Research, A. Krause, E. Brunskill, K. Cho, B. Engelhardt, S. Sabato, and J. Scarlett, Eds., vol. 202. PMLR, 23–29 Jul 2023, pp. 36 978–36 989. [Online]. Available: <https://proceedings.mlr.press/v202/weng23b.html>

[17] Q. Massoz, T. Langohr, C. François, and J. G. Verly, "The ulg multimodality drowsiness database (called drozy) and examples of use," in *2016 IEEE Winter Conference on Applications of Computer Vision (WACV)*. IEEE, 2016, pp. 1–7.

[18] A. Schwarz, M. Haurilet, M. Martinez, and R. Stiefelhagen, "Driveahead-a large-scale driver head pose dataset," in *Proceedings of the IEEE Conference on Computer Vision and Pattern Recognition Workshops*, 2017, pp. 1–10.

[19] M. Roth and D. M. Gavrila, "Dd-pose-a large-scale driver head pose benchmark," in *2019 IEEE Intelligent Vehicles Symposium (IV)*. IEEE, 2019, pp. 927–934.

[20] C. Zhao, B. Zhang, J. He, and J. Lian, "Recognition of driving postures by contourlet transform and random forests," *Iet Intelligent Transport Systems*, vol. 6, pp. 161–168, 2012. [Online]. Available: <https://api.semanticscholar.org/CorpusID:62754971>

[21] E. Ohn-Bar and M. M. Trivedi, "Hand gesture recognition in real time for automotive interfaces: A multimodal vision-based approach and evaluations," *IEEE transactions on intelligent transportation systems*, vol. 15, no. 6, pp. 2368–2377, 2014.

[22] A. Jain, H. S. Koppula, S. Soh, B. Raghavan, A. Singh, and A. Saxena, "Brain4cars: Car that knows before you do via sensory-fusion deep learning architecture," *arXiv preprint arXiv:1601.00740*, 2016.

[23] C.-H. Weng, Y.-H. Lai, and S.-H. Lai, "Driver drowsiness detection via a hierarchical temporal deep belief network," in *Computer Vision–ACCV 2016 Workshops: ACCV 2016 International Workshops, Taipei, Taiwan, November 20–24, 2016, Revised Selected Papers, Part III 13*. Springer, 2017, pp. 117–133.

[24] Y. Abouelnaga, H. M. Eraqi, and M. N. Moustafa, "Real-time distracted driver posture classification," *arXiv preprint arXiv:1706.09498*, 2017.

[25] W. Othman, A. Kashevnik, A. Ali, and N. Shilov, "Drivermv: In-cabin dataset for driver monitoring including video and vehicle telemetry information," *Data*, vol. 7, no. 5, 2022. [Online]. Available: <https://www.mdpi.com/2306-5729/7/5/62>

[26] K. Simonyan and A. Zisserman, "Two-stream convolutional networks for action recognition in videos," in *Advances in Neural Information Processing Systems 27: Annual Conference on Neural Information Processing Systems 2014, December 8–13 2014, Montreal, Quebec, Canada*, Z. Ghahramani, M. Welling, C. Cortes, N. D. Lawrence, and K. Q. Weinberger, Eds., 2014, pp. 568–576.

[27] D. Tran, L. Bourdev, R. Fergus, L. Torresani, and M. Paluri, "Learning spatiotemporal features with 3d convolutional networks," in *Proceedings of the IEEE international conference on computer vision*, 2015, pp. 4489–4497.

[28] J. Carreira and A. Zisserman, "Quo vadis, action recognition? A new model and the kinetics dataset," in *2017 IEEE Conference on Computer Vision and Pattern Recognition, CVPR 2017, Honolulu, HI, USA, July 21–26, 2017*. IEEE Computer Society, 2017, pp. 4724–4733. [Online]. Available: <https://doi.org/10.1109/CVPR.2017.502>

[29] J. Lin, C. Gan, and S. Han, "TSM: temporal shift module for efficient video understanding," in *2019 IEEE/CVF International Conference on Computer Vision, ICCV 2019, Seoul, Korea (South), October 27 - November 2, 2019*. IEEE, 2019, pp. 7082–7092. [Online]. Available: <https://doi.org/10.1109/ICCV.2019.00078>

[30] B. Zhou, A. Andonian, A. Oliva, and A. Torralba, "Temporal relational reasoning in videos," in *Computer Vision - ECCV 2018 - 15th European Conference, Munich, Germany, September 8–14, 2018, Proceedings, Part I*, ser. Lecture Notes in Computer Science, V. Ferrari, M. Hebert, C. Sminchisescu, and Y. Weiss, Eds., vol. 11205. Springer, 2018, pp. 831–846. [Online]. Available: [https://doi.org/10.1007/978-3-030-01246-5\\_49](https://doi.org/10.1007/978-3-030-01246-5_49)

[31] C. Feichtenhofer, H. Fan, J. Malik, and K. He, "Slowfast networks for video recognition," in *2019 IEEE/CVF International Conference on Computer Vision, ICCV 2019, Seoul, Korea (South), October 27 - November 2, 2019*. IEEE, 2019, pp. 6201–6210. [Online]. Available: <https://doi.org/10.1109/ICCV.2019.00630>

[32] G. Bertasius, H. Wang, and L. Torresani, "Is space-time attention all you need for video understanding?" in *Proceedings of the 38th International Conference on Machine Learning, ICML 2021, 18–24 July 2021, Virtual Event*, ser. Proceedings of Machine Learning Research, M. Meila and T. Zhang, Eds., vol. 139. PMLR, 2021, pp. 813–824. [Online]. Available: <http://proceedings.mlr.press/v139/bertasius21a.html>

[33] A. Arnab, M. Dehghani, G. Heigold, C. Sun, M. Lučić, and C. Schmid, "Vivit: A video vision transformer," in *Proceedings of the IEEE/CVF international conference on computer vision*, 2021, pp. 6836–6846.

[34] M. Patrick, D. Campbell, Y. M. Asano, I. M. F. Metze, C. Feichtenhofer, A. Vedaldi, and J. F. Henriques, "Keeping your eye on the ball: Trajectory attention in video transformers," in *Advances in Neural Information Processing Systems (NeurIPS)*, 2021.

[35] K. Li, Y. Wang, P. Gao, G. Song, Y. Liu, H. Li, and Y. Qiao, "Uniformer: Unified transformer for efficient spatial-temporal representation learning," in *The Tenth International Conference on Learning Representations, ICLR 2022, Virtual Event, April 25–29, 2022*. OpenReview.net, 2022. [Online]. Available: [https://openreview.net/forum?id=nBU\\_u6DLvoK](https://openreview.net/forum?id=nBU_u6DLvoK)

[36] Z. Tong, Y. Song, J. Wang, and L. Wang, "Videomae: Masked autoencoders are data-efficient learners for self-supervised video pre-training," *Advances in neural information processing systems*, vol. 35, pp. 10 078–10 093, 2022.

- [37] M. Wang, J. Xing, and Y. Liu, “Actionclip: A new paradigm for video action recognition,” *CoRR*, vol. abs/2109.08472, 2021. [Online]. Available: <https://arxiv.org/abs/2109.08472>
- [38] Y. Ma, G. Xu, X. Sun, M. Yan, J. Zhang, and R. Ji, “X-CLIP: end-to-end multi-grained contrastive learning for video-text retrieval,” in *MM '22: The 30th ACM International Conference on Multimedia, Lisboa, Portugal, October 10 - 14, 2022*. ACM, 2022, pp. 638–647. [Online]. Available: <https://doi.org/10.1145/3503161.3547910>
- [39] Y. Li, Y. Wang, W. Wang, D. Lin, B. Li, and K.-H. Yap, “Open world object detection: A survey,” *IEEE Transactions on Circuits and Systems for Video Technology*, 2024.
- [40] G. Elsayed, A. Mahendran, S. Van Steenkiste, K. Greff, M. C. Mozer, and T. Kipf, “Savi++: Towards end-to-end object-centric learning from real-world videos,” *Advances in Neural Information Processing Systems*, vol. 35, pp. 28 940–28 954, 2022.
- [41] F. Locatello, D. Weissenborn, T. Unterthiner, A. Mahendran, G. Heigold, J. Uszkoreit, A. Dosovitskiy, and T. Kipf, “Object-centric learning with slot attention,” *Advances in neural information processing systems*, vol. 33, pp. 11 525–11 538, 2020.
- [42] C.-Y. Wu and P. Krahenbuhl, “Towards long-form video understanding,” in *Proceedings of the IEEE/CVF Conference on Computer Vision and Pattern Recognition*, 2021, pp. 1884–1894.
- [43] X. Wang and A. Gupta, “Videos as space-time region graphs,” in *Proceedings of the European conference on computer vision (ECCV)*, 2018, pp. 399–417.
- [44] J. Wei, X. Wang, D. Schuurmans, M. Bosma, F. Xia, E. Chi, Q. V. Le, D. Zhou *et al.*, “Chain-of-thought prompting elicits reasoning in large language models,” *Advances in neural information processing systems*, vol. 35, pp. 24 824–24 837, 2022.
- [45] K. He, G. Gkioxari, P. Dollár, and R. Girshick, “Mask r-cnn,” in *Proceedings of the IEEE international conference on computer vision*, 2017, pp. 2961–2969.
- [46] Y. Chen, D. Chen, R. Liu, S. Zhou, W. Xue, and W. Peng, “Align before adapt: Leveraging entity-to-region alignments for generalizable video action recognition,” in *Proceedings of the IEEE/CVF Conference on Computer Vision and Pattern Recognition*, 2024, pp. 18 688–18 698.
- [47] W. Kay, J. Carreira, K. Simonyan, B. Zhang, C. Hillier, S. Vijayanarasimhan, F. Viola, T. Green, T. Back, P. Natsev *et al.*, “The kinetics human action video dataset,” *arXiv preprint arXiv:1705.06950*, 2017.